Detection of circumstellar material in a normal Type Ia Supernova

F. Patat[1*], P. Chandra[2,3], R. Chevalier[2], S. Justham[4], Ph. Podsiadlowski[4], C. Wolf[4], A. Gal-Yam[5], L. Pasquini[1], I.A. Crawford[6], P.A. Mazzali[7,8], A.W.A. Pauldrach[9] K. Nomoto[10], S. Benetti[11], E. Cappellaro[11], N. Elias-Rosa[7,12], W. Hillebrandt[7], D.C. Leonard[13], A. Pastorello[14], A. Renzini[11], F. Sabbadin[11], J.D. Simon[5], M. Turatto[11]

[1]European Southern Observatory, K. Schwarzschild Str.2, 85748, Garching b. München, Germany

[2]University of Virginia, Dept. of Astronomy, PO Box 400325, Charlottesville, VA 22904, USA

[3] Jansky Fellow, National Radio Astronomy Observatory

[4]Dept. of Astrophysics, University of Oxford, Oxford OX1 3RH, UK

[5]Astronomy Department, MS 105-24, California Institute of Technology, Pasadena, CA 91125,USA

[6]School of Earth Sciences, Birkbeck College London, Malet Street, London WC1E 7HX, UK

[7]Max-Planck-Institut für Astrophysik, K. Schwarzschild Str.1, 85748, Garching b. Muenchen, Germany

[8]INAF-Osservatorio Astronomico, v. Tiepolo 11, 34131 Trieste, Italy

[9]Institut für Astronomie und Astrophysik der Ludwig-Maximilians-Universität, 81679 Munich, Germany

[10]Dept. of Astronomy, University of Tokyo, Bunkyo-ku, Tokyo 113-0033, Japan

[11]INAF-Osservatorio Astronomico, v. Osservatorio 5, 35122 Padova, Italy

[12]Universidad de La Laguna, Av. Astrofísico Fransisco Sánchez s/n, E-38206, La Laguna, Tenerife, Spain

[13]Department of Astronomy, San Diego State University, San Diego, California 92182, USA

[14]Astrophysics Research Centre, Queen's University Belfast, BT7 1NN, UK

[*]To whom correspondence should be addressed. E-mail: fpatat@eso.org

ACCEPTED FOR PUBLICATION IN SCIENCE

(Submitted on March 26, 2007 - Accepted on June 29, 2007)

Type Ia supernovae are thought to be thermonuclear explosions of accreting white dwarfs that reach a critical mass limit. Despite their importance as cosmological distance indicators, the nature of their progenitors has remained controversial. Here we report the detection of circumstellar material in a normal Type Ia supernova. The expansion velocities, densities and dimensions of the circumstellar envelope indicate that this material was ejected from the progenitor system. The relatively low expansion velocities appear to favor a progenitor system where a white dwarf accretes material from a companion star which is in the red-giant phase at the time of explosion.

Due to their extreme luminosities and high homogeneity, Type Ia Supernovae have been used extensively as cosmological reference beacons to trace the evolution of the Universe *(1, 2)*. However, despite significant recent progress, the nature of the progenitor stars and the physics which govern these powerful explosions have remained very poorly understood *(3, 4)*. In the presently favored single-degenerate model, the supernova progenitor is a white dwarf in a close binary accreting from a non-degenerate companion *(5)*; the white dwarf explodes in a thermonuclear explosion when it approaches the Chandrasekhar limit. A direct method for investigating the nature of the progenitor systems of Type Ia supernovae (hereafter SNe Ia) is to search for signatures of the material transferred to the accreting white dwarf in the circumstellar material (CSM). Previous attempts have aimed at detecting the radiation which would arise from the interaction between the fast moving SN ejecta and the slow moving CSM in the form of narrow emission lines *(6)*, radio *(7)* and X-ray emission *(8)*. The most stringent upper limit to the mass loss rate set by radio observations is as low as 3×10^{-8} solar masses per year ($M_\odot$ yr^{-1}) for an assumed wind velocity of $10\,\mathrm{km\,s^{-1}}$ *(7)*. Two remarkable exceptions are represented by two peculiar SNe Ia, SN 2002ic and SN 2005gj, which have shown extremely pronounced hydrogen emission lines *(9, 10)*, that have been interpreted as a sign of strong ejecta-CSM

interaction *(11)*. However, the classification of these supernovae as SNe Ia has recently been questioned *(12)*, and even if they were SN Ia, they are unlikely to account for normal Type Ia explosions *(7)* that, so far, lack any signature of mass transfer from a hypothetical donor. Here, we report direct evidence of CSM in a SN Ia that has shown a normal behavior at X-ray, optical and radio wavelengths.

SN 2006X was discovered in the Virgo Cluster spiral galaxy NGC 4321 *(13)*. A few days later, the object was classified as a normal Type Ia event occurring $1-2$ weeks before maximum light, which was affected by substantial extinction *(14)*. Prompt Very Large Array (VLA) observations have shown no radio source at the SN position *(15)*, establishing one of the deepest and earliest limits for radio emission from a Type Ia, and implying a mass-loss rate of less than a few 10^{-8} $M_\odot$ yr^{-1} (for a low wind velocity of $10\,\mathrm{km\,s^{-1}}$). The SN was not visible in the 0.2–10 keV X-rays band down to the SWIFT satellite detection limit *(8)*.

We have observed SN 2006X with the Ultraviolet and Visual Echelle Spectrograph mounted at the European Southern Observatory 8.2m Very Large Telescope. Observations were carried out on four different epochs, which correspond to days -2, +14, +61 and +121 with respect to B-band maximum light. Additionally, a fifth epoch (day +105) was covered with the High Resolution Echelle Spectrometer mounted at the 10m Keck telescope *(16)*. The most remarkable finding from our data is the clear evolution seen in the profile of the Na I D lines (5889.95, 5895.92 Å). In fact, besides a strongly saturated and constant component, arising in the host galaxy disk (see section S2, Fig. S1), a number of features spanning a velocity range of about 100 km s^{-1} appear to vary significantly with time (Fig. 1, Fig. S2). SN 2006X is projected onto the receding side of the galaxy, and the component of the rotation velocity along the line of sight at the apparent SN location is about +75 km s^{-1} *(17)*, which coincides with the strongly saturated Na I D component, the saturated Ca II H&K lines, and a weakly saturated CN vibrational band (0-0) (Fig. 2, Fig. S1). This and the lack of time evolution proves that the deep absorption

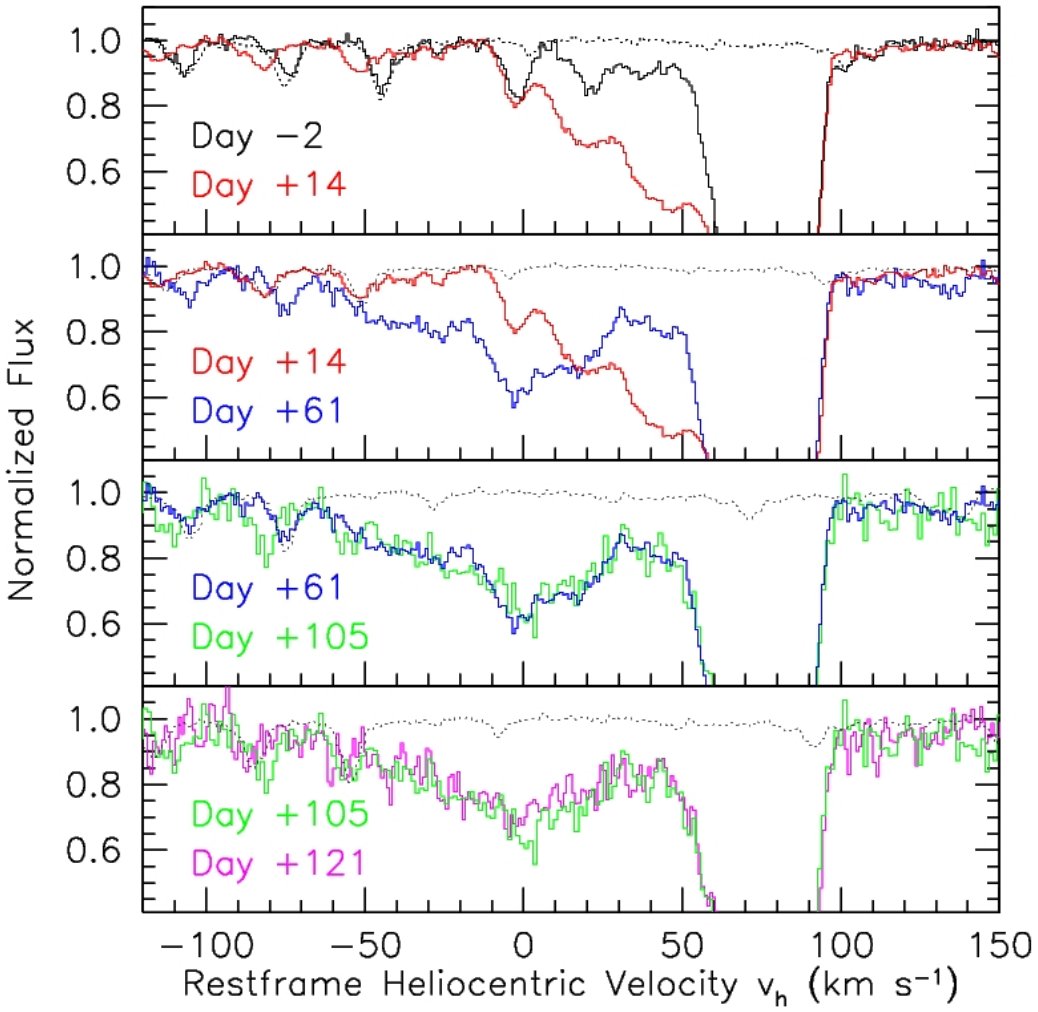

Figure 1: Time evolution of the Sodium D_2 component region as a function of elapsed time since B-band maximum light. The heliocentric velocities have been corrected to the rest-frame using the host galaxy recession velocity. All spectra have been normalized to their continuum. In each panel, the dotted curve traces the atmospheric absorption spectrum.

arises within the disk of NGC 4321 in an interstellar molecular cloud (or system of clouds) that is responsible for the bulk of the reddening suffered by SN 2006X (see text S2).

In contrast, the relatively blue-shifted structures of the Na I D lines show a rather complex evolution. The number of features, their intensity and width are difficult to establish. Nevertheless, for the sake of discussion, four main components, which we will indicate as A, B, C and D, can be tentatively identified in the first two epochs (Fig. 2). Components B, C and D strengthen between day -2 and day +14 while component A remains constant during this time interval. The situation becomes more complicated on day +61: components C and D clearly start to decrease in strength, but component B remains almost constant and component A becomes definitely deeper and is accompanied by a wide absorption that extends down to a rest-frame heliocentric velocity $v_h \simeq -50$ km s^{-1} (Fig. 1, Fig. S2). After this epoch there is no evidence of evolution, and component A remains the most intense feature up to the last phase covered by our observations, more than four months after the explosion.

Variable interstellar absorption on comparably short timescales has been claimed for some Gamma Ray Bursts (GRB), and it has been attributed by some authors to line-of-sight geometrical effects, due to the fast GRB expansion coupled to the patchy nature of the intervening absorbing clouds *(18)*. Our data clearly show that despite the marked evolution in the Na I D lines, Ca II H&K components do not change with time (see Fig. 2, Fig. S3 and the discussion in sections S3 and S4). Therefore, in the case of SN 2006X, transverse motions in the absorbing material and line-of-sight effects due to the fast SN photosphere expansion (typically 10^4 km s^{-1}) can be definitely excluded, since they would cause variations in all absorption features.

For this reason we conclude that the Na I features seen in SN 2006X, arising in a number of expanding shells (or clumps), evolve because of changes in the CSM ionization conditions induced by the variable SN radiation field. In this context, the different behavior seen in the Na I and Ca II lines is explained in terms of the lower ionization potential of Na I (5.1 eV,

corresponding to 2417Å) with respect to Ca II (11.9 eV, corresponding to 1045Å), their different recombination coefficients and photoionization cross sections coupled to a UV-deficient radiation field (see text S4). Regrettably, not much is known about the UV emission of SNe Ia shortwards of 1100Å *(8, 19)*. From a theoretical point of view, a severe UV line blocking by heavy elements like Fe, Co and Mg is expected *(20)*. An estimate of the Na I ionizing flux, S_{UV}, can be derived from a synthetic spectrum of a Type Ia SN at maximum light *(21)*, and this turns out to be S_{UV} $\sim$5$\times$10^{50} photons s^{-1}. One can verify that this flux is largely sufficient to fully ionize Na I up to rather large distances r_i $\sim$5$\times$10^{18} cm.

Nevertheless, since the recombination timescale τ_r must be of the order of 10 days, this requires an electron density n_e as large as 10^5 cm^{-3} (see section S4). Given the low abundance of any other element, such a high electron density can be produced only by partial hydrogen ionization. Due to the severe line blocking suffered by Type Ia SNe *(20)*, the flux of photons capable of ionizing H is very small ($\sim$4$\times$10^{44} photons s^{-1}) and this imposes that the gas where the Na I time-dependent absorptions arise must be confined within a few 10^{16} cm from the SN (see text S4). In a SN of this type, the flux in the 1120–2640 Å band decreases by a factor of ten in the first two weeks after maximum light *(8, 19)*. Since at a distance of $\sim$10^{16} cm from the SN the ionization timescale τ_i for Na I is much shorter than τ_r, the ionization fraction grows with time following the increase of the UV flux during the pre-maximum phase, while after maximum it decreases following the recombination timescale. This would explain the overall growth of the blue components' depth, as shown by our data, in terms of an increasing fraction of neutral Na, while the different evolution of individual components would be dictated by differences in the densities and distances from the SN. Moreover, once all the Na II has recombined (which should happen within a few τ_r, i.e. $\sim$1 month), there should be no further evolution, in qualitative agreement with the observations. Additionally, since the flux of photons that can ionize Ca II is more than four orders of magnitude less than in the case of Na I (see

section S4), the corresponding ionization fraction is expected to be of a few per cent only. Therefore, the recombination of Ca III to Ca II does not produce measurable effects on the depth of Ca II H&K lines, as it is indeed observed (see text S3).

The H mass ($M(\mathrm{H})$) contained in the shells generating the observed absorptions can be estimated from our observations after making some conservative assumptions. The Na I column density $N(\mathrm{NaI})$ deduced from the most intense feature (D, day +14) is $N(\mathrm{NaI}) \simeq 10^{12}\ \mathrm{cm}^{-2}$. Assuming that the material generating this component is homogeneously distributed in a thin spherical shell with radius $10^{17}\,\mathrm{cm}$, a solar Na/H ratio ($\log$ Na/H=$-$6.3) and complete Na recombination, an upper limit to the shell mass can be estimated as $M(\mathrm{H}) \leq 3 \times 10^{-4}\ M_{\odot}$ (this value is reduced by a factor 100 for material at about 10^{16} cm, the most likely distance for components C and D; see below). Even in the case of complete ionization, such a H mass would produce an Hα luminosity of $\sim$4$\times$10^{34} erg s^{-1}, which is two orders of magnitude below the 3-sigma upper limits set by our observations at all epochs (Table S2) and by any other SN Ia observed so far *(6)*. Therefore, the absence of narrow emission lines above the detection limit is not in contradiction with the presence of partially ionized H up to masses of the order of 0.01 $\mathrm{M}_{\odot}$.

However, photo-ionization alone cannot account for the fact that not all features increase in depth with time (Fig. 2). In fact, on day +61, components C and D turn back to the same low intensity they had on day -2. One possible explanation is that the gas is re-ionized by some other mechanism, like the ejecta-CSM interaction. In this case, the absorbing material generating components C and D must be close enough to the SN so that the ejecta can reach it in about one month after the explosion ($\sim$10^{16} cm for maximum ejecta velocities of 4$\times$10^{4} km s^{-1}). Similarly, in order not to be reached by the ejecta more than four months after, A, B and the broad high-velocity components must arise at larger distances ($>$5$\times$10^{16} cm). This scenario is not ruled out by the lack of radio emission from SN 2006X *(15)*. In fact, in the light of our

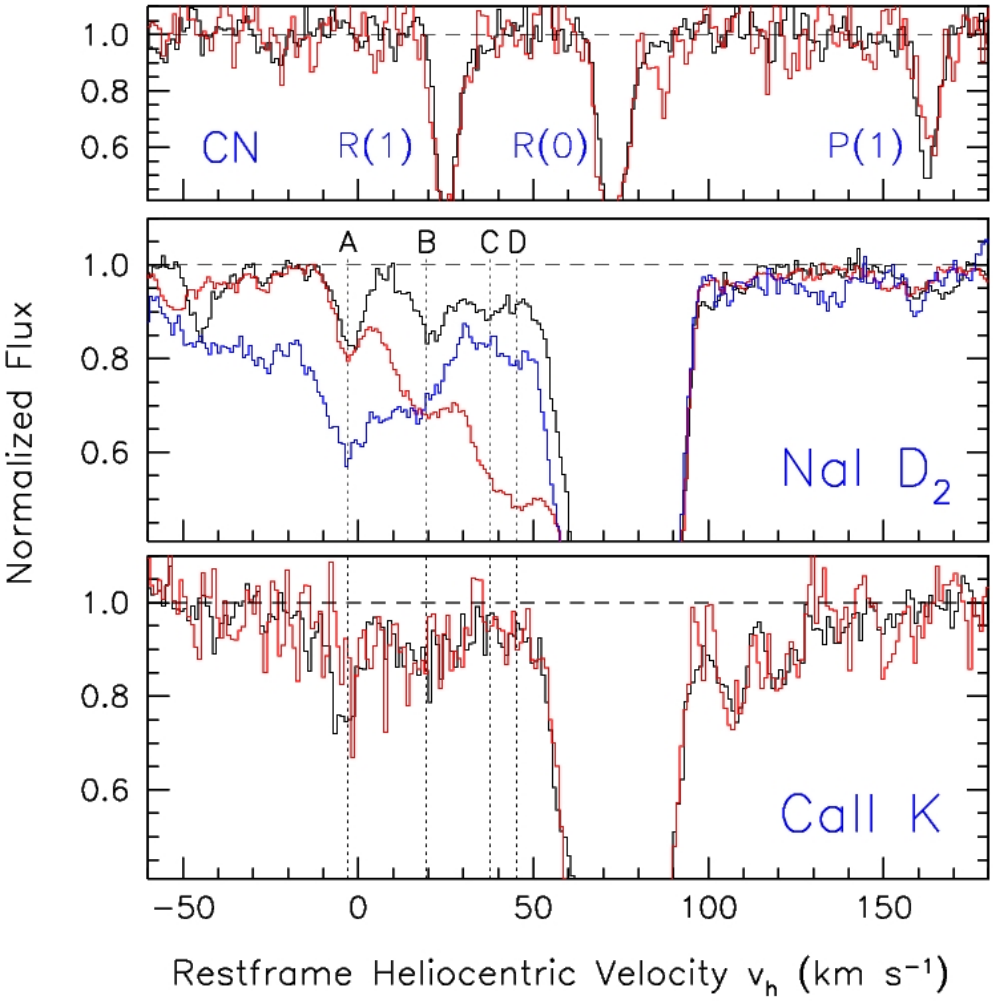

Figure 2: Evolution of the Na I D_2 and Ca II K line profiles between day -2 (black), day +14 (red) and day +61 (blue, Na I D_2 only). The vertical dotted lines mark the four main variable components at -3 (A), +20 (B), +38 (C) and +45 (D) km s^{-1}. For comparison, the upper panel shows the $R(0)$, $R(1)$ and $P(1)$ line profiles of the (0-0) vibrational band of the CN $B^2\Sigma - X^2\Sigma$. The velocity scale refers to the $R(0)$ transition (3874.608 Å). Color coding is as for the other two panels.

current understanding of the ejecta-CSM interaction mechanism *(22)*, the presence of similar shells with masses smaller than a few 10^{-4} $M_{\odot}$, cannot be excluded by radio non-detections of SNe Ia in general *(7)*. Our findings are consistent with upper limits on the radio flux set by our VLA observations, obtained about 10 months after the explosion (see section S1), which are comparable to the best upper limits set on the radio luminosity of other normal SNe Ia *(7)*.

If we adopt the velocity of the CN lines as indicative of the host galaxy rotation component along the line of sight at the SN location, then our observations provide solid evidence of CSM expanding at velocities that span a range of about 100 km s^{-1} (Fig. 2).

The most important implication of these observations is that they show that this circumstellar material was ejected from the progenitor system in the recent past. For instance, with a shell radius of 10^{16} cm and a wind velocity of $\sim$50 km s^{-1}, the material would have been ejected some 50 years before the explosion. This almost certainly rules out a double-degenerate scenario for SN 2006X, where the supernova would have been triggered by the merger of two CO white dwarfs. In this case, no significant mass loss would be expected in the phase immediately preceding the supernova. Thus, a single-degenerate model is the favored model for SN 2006X, where the progenitor accreted from a non-degenerate companion star.

Mean velocities for the circumstellar material of $\sim$50 km s^{-1} are comparable to those reported for the winds of early red giant (RG) stars *(22)*; velocities matching our observations are also expected for late subgiants. The observed material is moving more slowly than would be expected for winds from main sequence donor stars or from compact helium stars. Of the two major formation channels proposed for SN Ia with a non-degenerate donor star *(23)*, these wind velocities seem more consistent with the shorter-period end of the "symbiotic" formation channel. The observed structure of the circumstellar material could be due to variability in the wind from the companion RG; considerable variability of RG mass loss is generally expected *(24)*.

An alternative interpretation of these distinct features is that they arise in the remnant shells of successive novae, which can create dense shells in the slow moving material released by the companion *(25, 26)*. This seems to require an aspherical shell geometry in order to match the observed low velocities (see S6 for further details). Not only might this be expected a priori *(27)*, observations of the 2006 outburst of RS Ophiuchi show that there is an equatorial density enhancement which strongly restrains the expansion of the nova shell *(28, 29, 30)*.

One crucial issue is whether what we have seen in SN 2006X represents the rule or is rather an exceptional case. Other cases of SNe Ia showing negative velocity components are known, like SN 1991T and SN 1998es (see Fig. S5 and the discussion in S5). Unfortunately, multi-epoch high-resolution spectroscopy is not available for these objects (to our knowledge, the SN 2006X data set is unique in this respect), and therefore time variability cannot be demonstrated. Nevertheless, the data clearly show components approaching the observer at velocities which reach at least 50 km s^{-1} with respect to the deep absorption that we infer to be produced within the disks of the respective host galaxies. This, and the fact, that SN 2006X has shown no optical, UV and radio peculiarity whatsoever, supports the conclusion that what we have witnessed for this object is common to normal SN Ia, possibly all of them, even though variations due to different inclinations of the line of sight with respect to the orbital plane may exist.

References and Notes

1. A.G. Riess *et al.*, *Astron. J.* **116**, 1009 (1998).
2. S. Perlmutter *et al.*, *Astrophys. J.* **517**, 565 (1999).
3. D. Branch, M. Livio, L.R. Yungelson, F. Boffi, E. Baron, *Publ. Astr. Soc. Pac.* **107**, 1019 (1995).
4. W. Hillebrandt, J.C. Niemeyer, *Annu. Rev. Astron. Astrophys.* **38**, 191 (2000).
5. J. Whelan, I. Iben, *Astrophys. J.* **186**, 1007 (1973).
6. S. Mattila *et al.*, *Astron. Astrophys.* **443**, 649 (2005).
7. N. Panagia *et al.*, *Astrophys. J.*, **469**, 396 (2006).
8. S.I. Immler *et al.*, *Astrophys. J.* **648**, L119 (2006).
9. M. Hamuy *et al.*, *Nature* **424**, 651 (2003).

10. G. Aldering *et al.*, *Astrophys. J.*, **650**, 510 (2006).

11. The sub-luminous SN Ia 2005ke has shown an unprecedented X-ray emission, which has been interpreted as the signature of a possible weak ejecta-CSM interaction *(8)*. Nevertheless, this finding and the strong UV emission might be related to the nature of this SN.

12. S. Benetti *et al.*, *Astrophys. J.*, **653**, L129 (2006).

13. S. Suzuki, M. Migliardi, IAU Circ. **8667** (2006).

14. R. Quimby, P. Brown, C. Gerardy, CBET **421** (2006).

15. C.J. Stockdale *et al.*, CBET **396** (2006).

16. Materials, Methods, Text and Figures are available as supporting material on *Science* online.

17. R.J. Rand, *Astrophys. J.* **109**, 2444 (1995).

18. H. Hao *et al.*, *Astrophys. J.* **659**, L99 (2007).

19. N. Panagia, *Supernova 1987A: 20 Years after: Supernovae and Gamma-Ray Bursters*, S. Immler, R. McCray and K.W. Weiler, Eds. (AIP Conf. Proc., 2007), in press; preprint available online (http://arxiv.org/abs/0704.1666).

20. W.A. Pauldrach *et al.*, *Astron. Astrophys.* **312**, 525 (1996).

21. R.A. Chevalier, C. Fransson, *Supernovae and Gamma-Ray Bursters*, K. Weiler, Ed. (Lecture Notes in Physics, vol. 598, Springer Verlag, New York, 2003), pp.171-194.

22. P.G. Judge, R.E. Stencel, *Astrophys. J.* **371**, 357 (1991).

23. I. Hachisu & M. Kato, *Astrophys. J.* **558**, 323 (2001).

24. L.A. Willson, *Ann. Rev. Astron. Astrophys.* **38**, 573 (2000).

25. I. Hachisu, M. Kato, *Astrophys. J.* **558**, 323 (2001).

26. W.M. Wood-Vasey, J.L. Sokoloski, *Astrophys. J.* **645**, L53 (2006).

27. I. Hachisu, M. Kato, K. Nomoto, *Astrophys. J.* **522**, 487 (1999).

28. T.J. O'Brien *et al.*, *Nature* **442,** 279 (2006).

29. M.F. Bode *et al.*, *Astrophys. J.* **652**, 629 (2006).

30. M.F. Bode, *et al.*, *Astrophys. J.*, in press; preprint available online (http://arxiv.org/abs/0706.2745).

31. We wish to thank K. Krisciunas for providing us with the information about the photometric evolution of SN 2006X. We acknowledge Katrien Steenbrugge, Francesca Primas, Michael Wood-Vasey, Romano Corradi, Gary J. Ferland, Peter van Hoof, Fabio Bresolin and Christopher Stockdale for useful discussions. We particularly thank M.F. Bode for sharing some results on RS Oph before publication. This work is based on observations made with ESO Telescopes at Paranal Observatory, obtained under Run IDs 276.D-5048, 277.D-5003 and 277.D-5013. Some of the data presented herein were obtained at the W.M. Keck Observatory, which is operated as a scientific partnership among the California Institute of Technology, the University of California and the National Aeronautics and Space Administration. This work made use of the Very Large Array telescope of the National Radio Astronomy Observatory, which is operated by Associated Universities, Inc. under a cooperative agreement with the National Science Foundation.

Supporting Online Material

S1. Materials and Methods

We have observed SN 2006X on 5 epochs spanning about 4 months (Table S1). High resolution spectra were obtained with the European Southern Observatory's (ESO) Very large Telescope (VLT) on Cerro Paranal (Chile), equipped with the Ultraviolet and Visual Echelle Spectrograph (UVES) *(S1)*, and with the Keck I Telescope equipped with the High Resolution Echelle Spectrometer (HIRES) *(S2)*. For UVES we have used the 390+580 setting, which covers simultaneously three wavelength ranges (3290-4500Å, 4780-5740Å and 5830-6800Å), with a full width half maximum (FWHM) resolution of 7 km s^{-1}. In the case of HIRES, we have used a setting optimized for the NaI D region, that covers the wavelength range 3900-8350Å with a FWHM resolution of 6.8 km s^{-1}. UVES data have been reduced using the UVES Data Reduction Pipeline *(S3)*, while HIRES data have been processed using standard procedures for Echelle spectra. Wavelength calibration has been achieved using Thorium-Argon lamps. The final RMS accuracy is about 0.15 km s^{-1}. The wavelength scale was corrected to the rest-frame adopting a host galaxy recession velocity of 1571 km s^{-1} *(S4)*. To compensate for the Earth's motion, a heliocentric velocity correction has been applied to the data (Table S1). The effect of atmospheric lines has been checked using a spectroscopically featureless bright star (HR 3239) observed with the same instrumental setup as for the science data. The spectral region of interest turns out to be essentially free of telluric features. Therefore, the broad absorption visible starting with day +61 and reaching $v_h \sim -70$ km s^{-1} is real and not affected by atmospheric lines. Na I column densities have been estimated fitting Voigt line profiles with VPFIT *(S5)*. Finally, epochs have been computed from B maximum light, which took place on February 20, 2006 *(S6)*.

In order to set upper limits to Hα and He I 5876Å luminosities (Table S2), the UVES spectra have been calibrated by means of a reference response function. Since the observations have been obtained under sky transparency conditions that ranged from clear/photometric (epochs -2, +14, and +121) to thin cirrus (+61), taking into account the high instrument stability, the expected flux calibration accuracy is of the order of 20-30%. To the best of our knowledge, the upper limits on Hα and He I 5876Å presented here are the latest ever published. The signal-to-noise ratio on the continuum in the Na I D lines region ranges from $\sim$70 (day -2) to $\sim$20 (day +121).

To confirm the low mass of CSM estimated from the Na I observations, we have observed SN 2006X with the Very Large Array *(S8)*, in the C configuration, at 6 cm (4.8 GHz) on November 17 and at 3.6 cm (8.4 GHz) on November 20, 2006, corresponding to +270 and +273 days after B maximum light, respectively. The SN was not detected at both wavelengths, and the 2 SD limits are 0.07 mJy and 0.09 mJy for the two bands respectively *(S9)*, which are comparable to the best limits available so far *(S10)*. At the epoch sampled by our observations, the SN ejecta have reached a distance of $\sim 10^{17}$ cm from the explosion site. Our upper limits on the radio flux

UT Date (2006)	Phase (days)	Instrument/Telescope	Total Integration Time (seconds)	Heliocentric Correction (km s^{-1})
18/02	-2	UVES/VLT	4175	+14.6
06/03	+14	UVES/VLT	8940	+7.2
22/04	+61	UVES/VLT	15025	-15.4
06/06	+105	HIRES/KECK	3600	+5.0
25/06	+121	UVES/VLT	15025	-28.0

Table S1: High resolution spectroscopic observations of SN 2006X. Phase refers to B-band maximum light, attained on February 20, 2006 *(S6)*

constrain the corresponding CSM mass to be smaller than a few 10^{-3} solar masses ($M_\odot$), which is fully consistent with the estimates deduced from the observed Na I absorptions. Very similar upper limits have been set for standard SN Ia events like SN 1981B, 1989M, 1998bu and 1992A *(S10)*.

From the low resolution spectroscopic data that we have obtained in parallel to the high resolution data set discussed in this paper, we confirm the results of the early classification spectroscopy (S11). SN 2006X appears to be a normal Ia, very similar to SN 2002bo *(S12)*, with somewhat higher photospheric velocities. The derivation of photometric parameters is hindered by a rather strong reddening ($E(B-V)$ >1.1) and an anomalous extinction law (R_V <2). However, the decline rate, the light and color curve shapes and the absolute magnitude are within the range of normal Type Ia SNe *(S6)*.

S2. The interstellar material

The apparent position of SN 2006X is very close to a spiral arm of NGC 4321, which is inclined by 28 degrees with respect to the line of sight *(S13)*. Due to the relatively high extinction *(S11)*, the SN most likely exploded within or behind the disk of the host galaxy. Moreover, the SN is projected onto the receding side of the galaxy, and the component of the rotation velocity along the line of sight at the apparent SN location is about 75 km s^{-1} *(S4, S13)*, which coincides with the strongly saturated Na I D component (Fig. S1). This suggests rather unequivocally that the time-invariant, very deep absorptions arise within the disk of NGC 4321. The equivalent widths of the Na I D lines, measured in the first epoch spectrum, are 670±5 and 625±4 mÅ for the D_2 and D_1 components respectively. The implied total Na I column density, estimated fitting multiple Voigt line profiles with VPFIT *(S5)*, is as large as $\log N$ ∼14.3. For a Milky Way-like dust mixture this would turn into a color excess E_{B-V} ∼1.1 *(S14)*. Moreover, the CN lines clearly visible in our first two spectra at v_h=73.6±1.0 km s^{-1} (weighted average of the two epochs) have an unprecedented depth (see also ref. *S15)*. On the first epoch spectrum the equivalent widths for the three lines are: $EW[R(0)]$=91±2, $EW[R(1)]$=60±3 and $EW[P(1)]$=42±3 mÅ that, after correcting for saturation effects, correspond to column

Phase	Hα		He I 5876	
	7 km s^{-1}	50 km s^{-1}	7 km s^{-1}	50 km s^{-1}
-2	2.2	16.0	2.4	17.0
+14	1.1	8.0	1.1	7.6
+61	0.6	4.0	0.6	4.4
+121	0.3	2.2	0.4	2.6

Table S2: Upper limits (3 SD) for Hα and He I 5876Å luminosities measured on the UVES spectra. Luminosities are expressed in 10^{37} erg s^{-1} and were computed for two Gaussian line profiles with FWHM 7 km $^{-1}$ (matching the instrumental resolution) and 50 km s^{-1}, assuming a distance of 16.1 Mpc for NGC 4321 *(S7)*.

densities of $\log[N_{R(0)}]$=14.0$\pm$0.1, $\log[N_{R(1)}]$=13.6$\pm$0.1 and $\log[N_{R(1)}]$=13.6$\pm$0.1 respectively. Stars having comparable column densities in our own Galaxy are known to have color excesses larger than E_{B-V}=1 *(S16)*. Applying the usual curve of growth method *(S16)*, an excitation temperature of 3.0 $\pm$ 0.2 °K is derived for this cloud.

A closer inspection of Fig. S1 shows that the deep Na I and Ca II absorptions are not due to a single cloud. In fact the Ca II H line, which is less affected by saturation, clearly displays at least two components that differ in velocity by $\sim$10 km s^{-1}. On the contrary, the CN lines appear as single, unresolved features (the velocity dispersion parameter is b $\sim$2.3 km s^{-1}), indicating that this molecular absorption arises within an inner subset (as seen along the line of sight) of multiple clouds that most likely contribute to the strong Na I and Ca II absorptions.

The peculiarity of the interstellar material is indicated also by the unusual wavelength dependency of the continuum linear polarization shown by SN 2006X. This is in fact significantly different from that typically observed in extinguished stars within our own Galaxy *(S18)*.

The presence of strongly saturated Na ID interstellar components could in principle mask the existence of weaker features, which happen to fall in the same velocity range but arise in a completely different region. Therefore, the presence of an absorption feature at the typical velocity of a RG wind (10 km s^{-1}) cannot be ruled out. Only the study of non-extinguished objects, i.e. free of strong interstellar absorptions, will allow us to detect slow moving material in the surroundings of Type Ia SNe.

S3. Lack of evolution in Ca II H&K lines

The NaI D evolution is very clearly displayed by both D_1 and D_2 lines, which show practically identical profiles at all epochs (Fig. S2). Slight saturation effects are visible in the most intense components of the D_2 line.

The behavior of the Ca II H & K lines is radically different from that of the Na I D lines. On the first epoch (day -2), the profiles of Na I D_2 and Ca II K show very similar intensity and velocity profiles (Fig. S3). In particular, components A and B can be easily identified. The

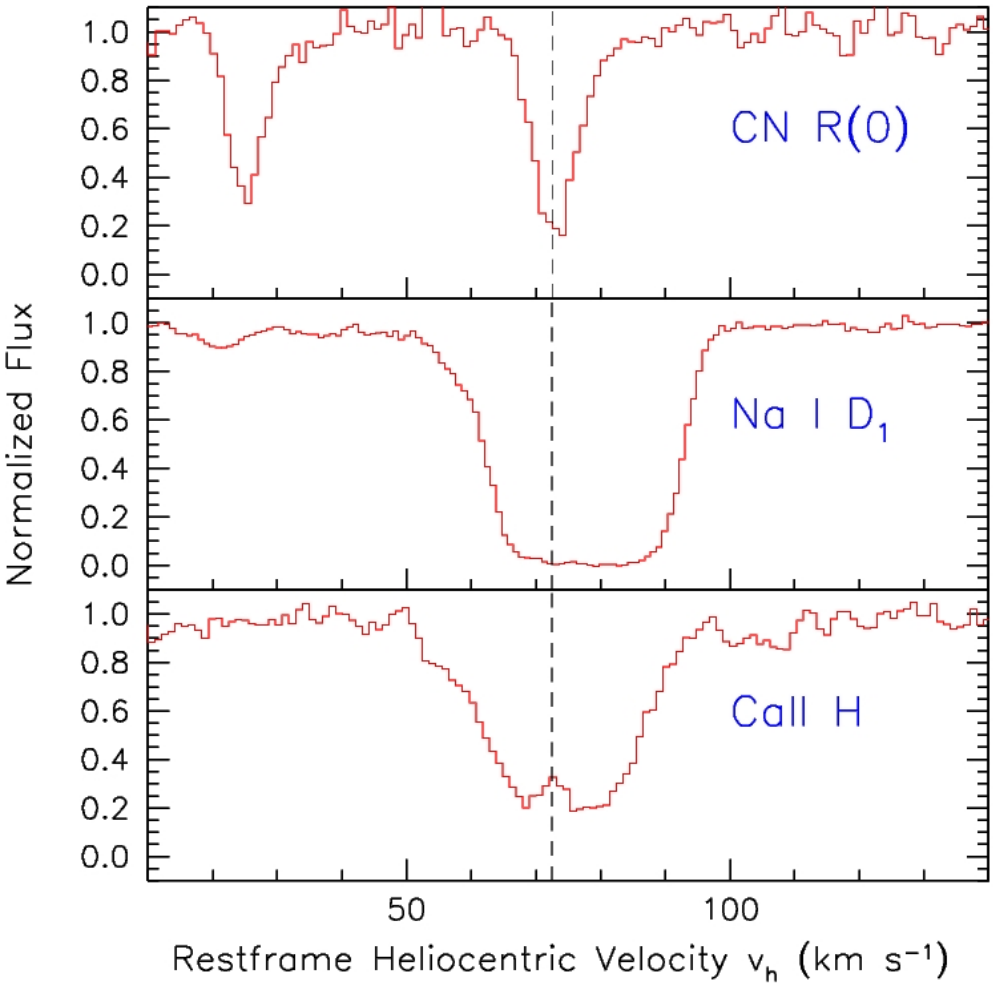

Figure S1: Comparison between the profiles of CN R(0), Na I D_1 and Ca II K lines for the first UVES epoch (day -2). The vertical dashed line marks the velocity of the R(0) absorption center (v_h=73.6 km s^{-1}).

differences become dramatic at the second epoch (day +14), when Ca II K remains practically unchanged while Na I D_2 develops deep absorptions for components B, C and D. The signal-to-noise ratio in the Ca II region is lower, but a variation similar to that taking place for the Na I lines would have been definitely detected, at least for components B, C and D. Due to the SN fading and its spectral evolution, the continuum in the Ca II H&K region becomes very weak as time goes by, making the detection of the K line more and more difficult. Even heavily binning our third epoch data (day +61), the signal-to-noise ratio achieved on the resulting profile is not sufficient to draw any firm conclusion (Fig. S3). At later epochs, due to the very low SN continuum, the H&K lines could not be detected.

Geometric effects related to the fast expansion of the radiation ring and the consequent change in the covering factor coupled to the patchy structure of the intervening absorbing clouds, have been advocated to explain the time variability claimed for some Gamma Ray Bursts (GRB) *(S19, S20)*. What emerges from this analysis is that a Ca II H&K evolution at the level seen in the Na I D lines can be definitely excluded. In turn, this rules out transverse motions or line-of-sight effects as responsibles for the evolution observed in SN 2006X.

S4. The location of the absorbing material in SN 2006X

After sodium is ionized by the SN radiation field, which drops quickly after maximum light *(S21)*, it starts recombining with a time scale τ_r which depends on the electron number density n_e and the radiative recombination coefficient β: $\tau_r = (n_e\ \beta)^{-1}$. Given the time scale of the observed changes in the NaID features, we estimate τ_r $\sim$10 days, which implies $n_e \sim 10^5$ cm^{-3} for $\beta \simeq 5\times10^{-12}$ cm^3 s^{-1} *(S22)*. Such an high electron density can only come from partial ionization of hydrogen. Therefore, the maximum distance for the gas where the time-variable NaI features arise is dictated by the ability of the SN to ionize hydrogen, i.e. by the flux S_{UV} of photons at wavelengths shorter than 912Å, times the duration Δt_{SN} of the UV emitting phase.

An upper limit to the number of hydrogen atoms that are ionized is therefore given by the total number of ionizing photons, $S_{UV}\Delta t_{SN}$, which in turn must be equal to $V_H\ n_e$, with V_H being the volume of the layer responsible for the varying absorption. Thus, an upper limit to this volume is given by:

$$V_H \leq \frac{S_{UV}\Delta t_{SN}}{n_e}. \qquad (S1)$$

Assuming that the absorbing material is confined within a thin shell of thickness Δr (with $\Delta r \ll r_H$), the maximum radius of such a shell is:

$$r_H \leq \left[\frac{S_{UV}\ \Delta t_{SN}}{4\pi\ n_e\ \Delta r/r}\right]^{1/3}. \qquad (S2)$$

Using S_{UV}= 4.4$\times10^{44}$ photons s^{-1}, the value derived from the synthetic spectrum at maximum light *(S23)*, and a light curve width of Δt_{SN}= 20 days, one gets r_H $\leq$4$\times10^{15}$ cm for

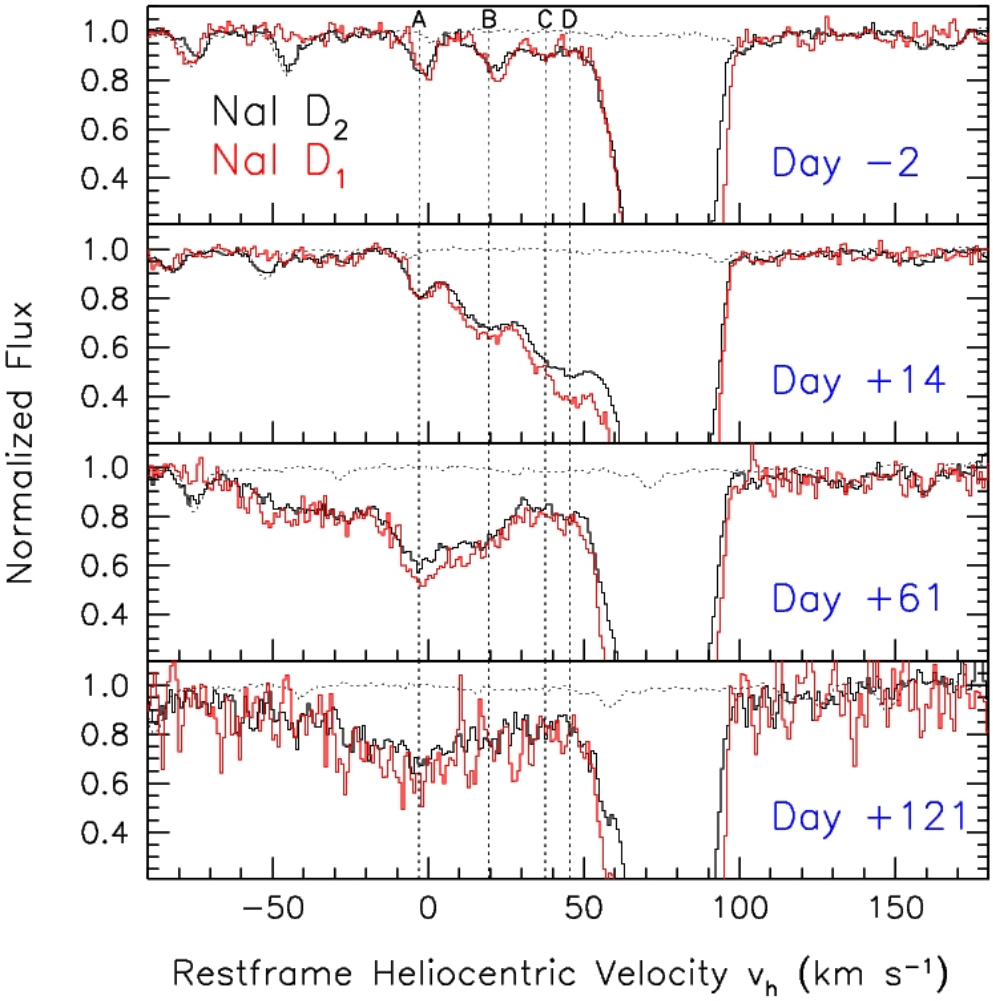

Figure S2: Comparison between the NaI D_1 and D_2 line profiles on days -2, +14, +61 and +121. For presentation, the intensity of the D_1 line has been multiplied by 2.0, that is the D_2/D_1 ratio expected from the spin orbit statistical weights of the Na($^2P_{3/2}$) and Na($^2P_{1/2}$) transitions. In each panel, the dotted curve traces the atmospheric absorption spectrum in the D_2 region. In order to account for the different heliocentric corrections applied to the SN data, the telluric absorption spectrum has been shifted in velocity to match the atmospheric features visible in the SN spectra. The vertical dashed lines mark the main velocity components.

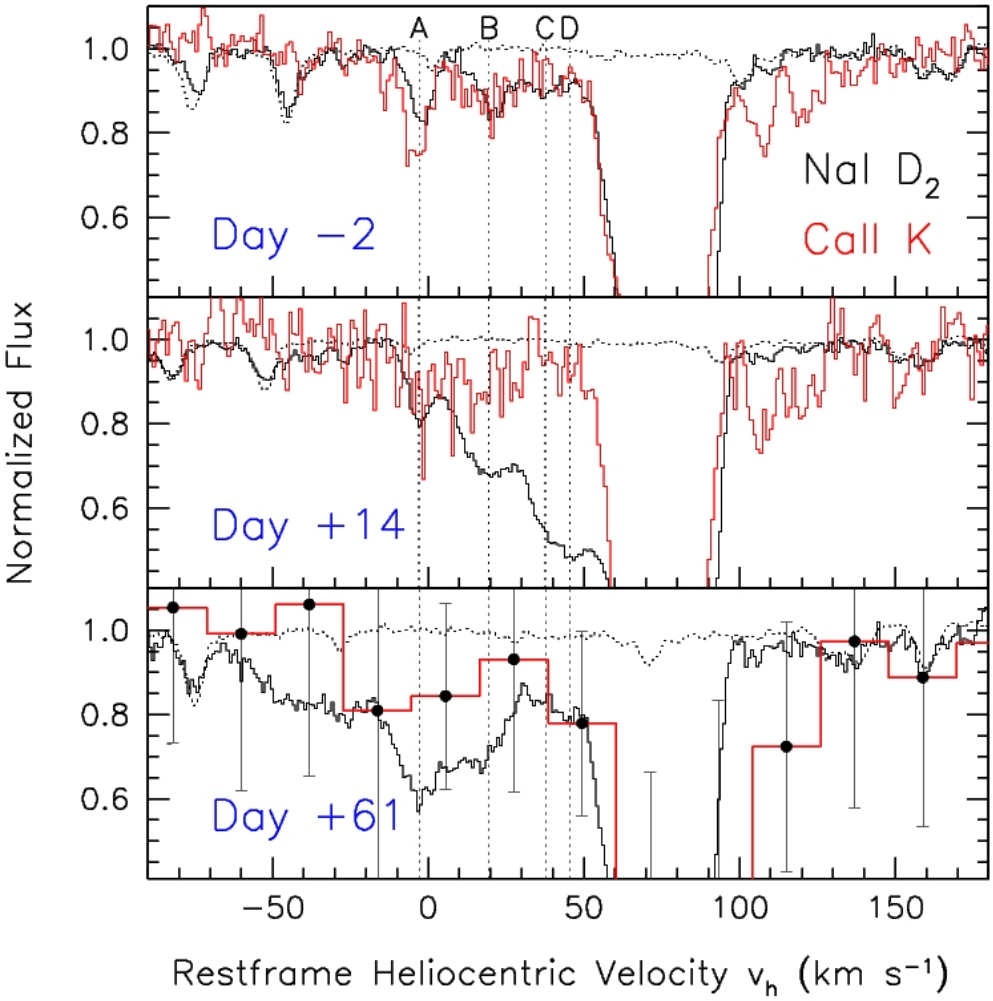

Figure S3: Comparison between the evolution of NaI D_2 and Ca II K lines during the first three epochs covered by our observations. In order to increase the signal-to-noise ratio on day +61 the Ca II K data have been binned to a 0.3 Å step, corresponding to about 23 km s^{-1}. The error bars indicate ± 1 SD level, estimated from the data within each single bin, composed by 21 original data points. In each panel, the dotted curve traces the atmospheric absorption spectrum in the D_2 region.

n_e=10^5 cm^{-3} and $\Delta r/r$=0.01. The largest uncertainty in estimating r_H comes from the total fluence of ionizing photons ($S_{UV}\Delta t_{SN}$). In fact, the synthetic spectrum we have used is a best fit to an HST spectrum of SN 1992A extending down to about 1600Å and obtained 6 days past maximum light and *(S24)*, i.e. when the UV flux has significantly dropped *(S21)*. Nevertheless, thanks to the cubic root dependency on it, even a 10^3 times higher fluence would result in an upper limit of $\sim 5\times10^{16}$ cm. This clearly demonstrates that the material responsible for the time-variable features is confined well within the circum-stellar domain.

This creates a very marked distinction between Type Ia SNe and GRBs, for some of which time-dependent UV absorption features have been claimed *(S19, S20, S25)*. In fact, GRBs and their early after-glows have a very strong X-ray/UV radiation field, so that all possible circumstellar gas is completely ionized. For instance, GRB 021004 was shown to be able to completely ionize the interstellar material out to about 100 pc ($\sim 3\times10^{20}$ cm) *(S19)*, while for GRB 060418 the ionization was found to reach $\sim$1.7 kpc ($\sim 5\times10^{21}$ cm) *(S25)*.

As far as calcium is concerned, we note that the flux of photons capable of ionizing Ca II computed from the synthetic spectrum *(S23)* is $\sim 3.5\times10^{46}$ photons s^{-1}. This is more than four orders of magnitude smaller than the corresponding Na I ionizing flux. As a consequence, the ionization fraction of Ca II is significantly smaller and hence, as it recombines, no detectable effect on the depth of Ca II H&K lines is expected, as shown by the observations (see S3 and Fig. S3). The same mechanism has been proposed to explain the inter-stellar line variability observed in galactic stars which, due to the much lower densities, takes place on timescales of years to decades *(S26)*.

An alternative explanation for the presence of expanding shells in the immediate surroundings of SN 2006X is that they have been lost by a nearby star, physically not related to the progenitor system but close enough to be influenced by the SN radiation field. In fact, shells expanding with velocities up to several tens of km s^{-1} are known to be present, for instance, around many galactic OB associations *(S26)*. Since the material has to be relatively close to the SN in order to be influenced by its UV radiation, this alternative scenario requires that the SN exploded within a cluster or a star association.

In order to study the immediate surroundings of the explosion site, we have used a deep pre-explosion image obtained with the ESO-VLT FOcal Reducer and low dispersion Spectrograph (FORS1), *(S28)*. Observations were performed on May 12, 1999 in the R passband *(S28)*, with an exposure time of 600 seconds and a seeing of 0.8 arcsec (FWHM), corresponding to a limiting magnitude $R\sim$24.0 (5 SD level) at the SN location (Fig. S4, left panel). To better characterize the SN environment, we have searched the Hubble Space Telescope Archive for high resolution imaging. The only suitable data we could find were obtained with the Advanced Camera for Surveys (ACS), *(S29)* on May 21, 2006 *(S30)* in high resolution mode (0.027 arcsec pixel^{-1}) with the F435W (1480 seconds), F555W and F775W (1080 seconds) filters. In order to increase the signal-to-noise ratio, the three images have been registered and stacked (Fig. S4, right panel). The resulting image reveals a wealth of resolved objects, which can be identified as red, blue super-giants, groups of O stars and OB associations, with typical sizes of $\sim$100 pc. All such associations and stellar groups (like those marked with labels A and B on the ACS

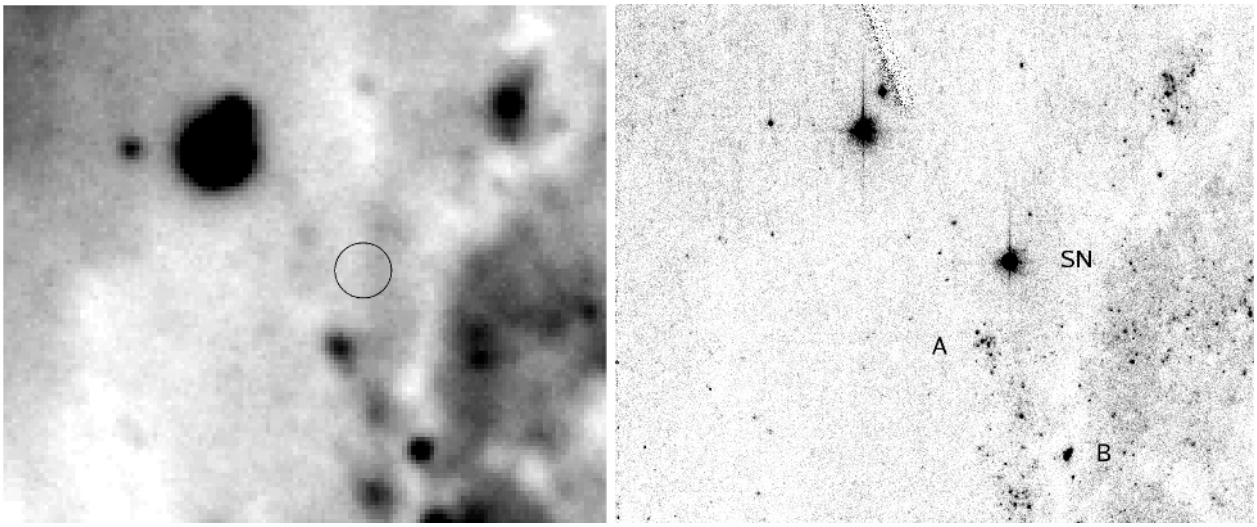

Figure S4: The host galaxy imaged before (left, VLT-FORS1) and after (right, HST-ACS) the explosion of SN 2006X. The field of view is 26.5×22.5 arcsec for both images. The SN position in the FORS1 image is marked by a circle. The spatial scale on the ACS images is about 2.1 pc pixel^{-1}.

image) are clearly detected in the deep FORS1 image, which shows also some of the brightest single stars.

Unfortunately, the ACS image was obtained after the explosion, when the SN was still bright, and hence it is not possible to directly inspect the SN surroundings. Nevertheless, the presence of groups like that marked with A in Fig. S4 can be excluded. This is confirmed by the deep FORS1 pre-explosion image, which does not show any trace of stellar associations (like A) or even more compact groups (like B) at the SN location. This makes the presence of an isolated star losing material in the immediate vicinity of the SN progenitor system very unlikely.

S5. Evidences of blue-shifted Na I absorption lines in other SNe Ia

Due to the large required exposure times, high resolution spectroscopy of SN Ia is rather rare. Additionally, since the main aim of those investigations was the study of the supposedly time-invariant inter-stellar medium, data were usually obtained on one single epoch around maximum light *(S31, S32)*. Only in recent times, with the advent of 8-10m class telescopes, multi-epoch high resolution spectroscopy has been performed, with the aim of detecting possible emission lines produced by the SN ejecta-CSM interaction *(S33, S34)*. Nevertheless, due to the underlying scientific driver of these projects, observations were carried out during the pre- and near-maximum phase, when the Na I D features are at their minimum intensity in SN 2006X

(Fig. S1). For example, the spectra of SN 2001el, observed some days before maximum light, do not show any clear signs of Na I D blue components. Interestingly, they do show at least two blue components in the Ca II H profile at ~ -18 and -34 km s^{-1} with respect to the deep Na I D absorption *(S33)*.

In the course of our long term nearby SN monitoring, we had the chance to obtain high resolution spectroscopy of two SN Ia, namely SN 1991T *(S35)* and SN 1998es *(S36)*. Both spectra are unpublished. SN 1991T was observed on Jun 08, 1991 (day +40) with the ESO 1.4m Coudè Auxiliary Telescope (CAT) equipped with the Coudè Echelle Spectrograph *(S37)*, while the spectrum of SN 1998es was obtained on Nov 24, 1998 (day -1) with the ESO 1.5m telescope equipped with the Fiber-fed Extended Range Optical Spectrograph *(S38)*. The Na I D line profiles of these two objects are remarkably similar to that of SN 2006X (Fig. S5). Besides a strong absorption, which is most likely generated within the disk of the host galaxy, some blue components are clearly visible.

To the best of our knowledge, the only other SN for which a data set somewhat similar to that of SN 2006X has been obtained is the core-collapse, Type IIn SN 1998S *(S39)*. High resolution spectroscopy of this object has revealed a number of Na I D components within the host galaxy, the bluest of which ($v_h \sim -100$ km s^{-1}) deepened significantly during the 19 days spanned by the two epochs available, implying a Na I column density increase of about 1 dex. This fact, together with the detection of time-evolving narrow H and He P-Cyg profiles at the same Na I velocity, was interpreted as a signature of the outflows from the super-giant progenitor of SN 1998S, arising in a dense shell, expanding at about 50 km s^{-1} *(S39, S40)*.

S6. The CSM structure around SN 2006X: swept-up nova shells?

A possible interpretation of the distinct features in the CSM is that they arise in the remnant shells of successive novae *(S41)*. The recurrent ejection of a few 10^{-7} M$_\odot$ of H at velocities of $\sim$4000 km s^{-1} can create dense shells in the slow moving material released by the companion, evacuating significant volumes around the progenitor system *(S42)*. This explanation requires that the high-velocity nova ejecta have, by sweeping up the stellar wind of the donor star, been slowed down to speeds several times lower than the asymptotic shell velocities seen, for instance, in RS Ophiuchi, i.e. $\sim 300\,\mathrm{km\,s^{-1}}$ *(S43, S44)*. For SN 2006X, if we assume that the observed shells have all been swept up in the energy-conserving phase *(S45)*, and if we take an upper limit of the wind-mass loss rate from the companion, $\dot{M}_{\rm wind}$, as $10^{-7}\ M_\odot$ yr^{-1} from the radio observations, we obtain an upper limit on the mass ejected in each nova outburst:

$$M_{\rm nova} < 2 \times 10^{-8}\, M_\odot \frac{\dot{M}_{\rm wind}}{10^{-7} M_\odot\,\mathrm{yr^{-1}}} \left(\frac{V_{\rm shell}}{75\,\mathrm{km\,s^{-1}}}\right)^2 \left(\frac{V_{\rm nova}}{1000\,\mathrm{km\,s^{-1}}}\right)^{-2} \frac{\Delta t_{\rm nova}}{10\,\mathrm{yr}}, \qquad \text{(S3)}$$

where M and V refer to mass and velocity, and the subscripts $nova$ and $shell$ refer to the mass ejected in each nova outburst and the shell formed as the nova ejecta sweep up the wind, whilst $\Delta t_{\rm nova}$ represents the nova recurrence time.

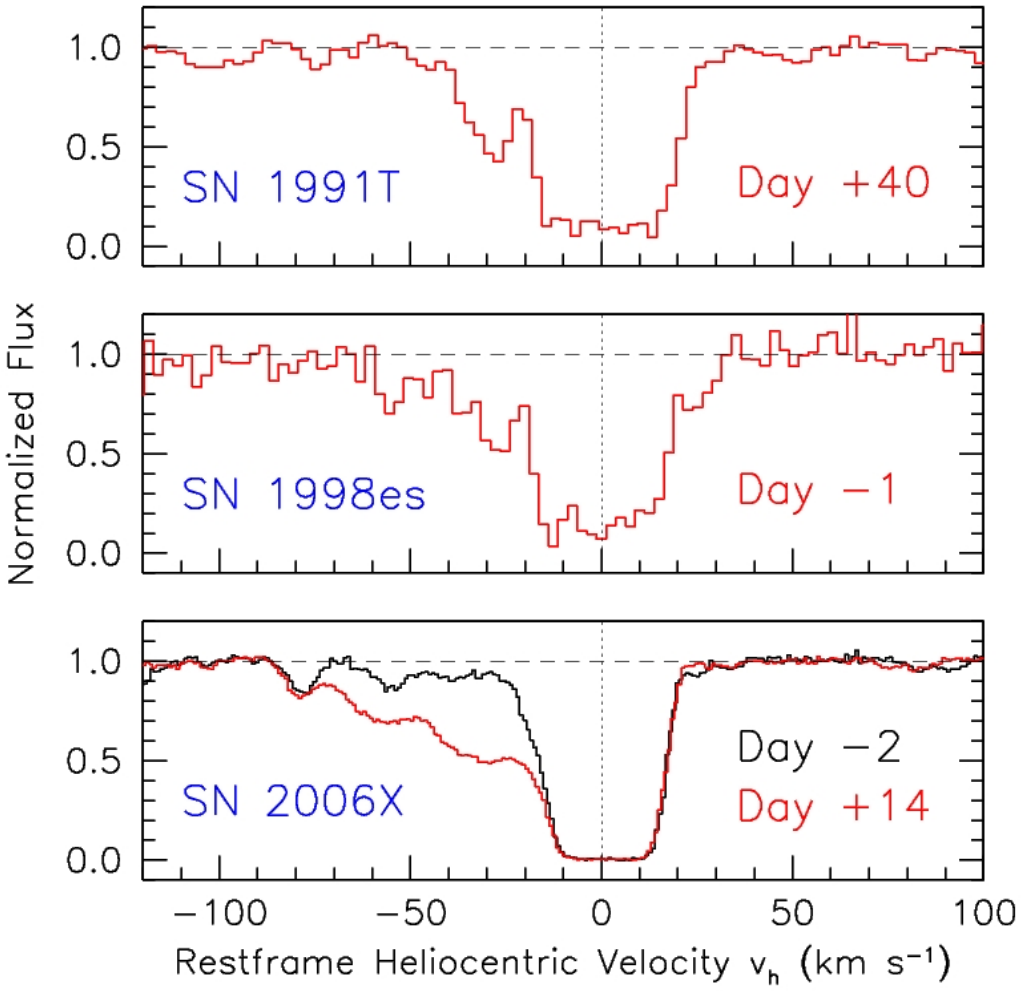

Figure S5: Comparison between the Sodium D_2 line profiles for three SN Ia: 1991T (upper), 1998es (middle) and 2006X (lower). For the sake of clarity, spectra have been arbitrarily shifted in the horizontal direction in order to place the center of the strongest D_2 component at zero velocity.

Although this value is around an order of magnitude smaller than might be expected from recent nova calculations, we note that the ejecta mass is a steeply decreasing quantity as the white dwarf approaches explosion *(S41, S46)*. In addition, the estimate above assumes that the wind from the companion is spherically symmetric. If the wind is concentrated towards the orbital plane, and if we are observing the shell structure close to the orbital plane, the shells in our line-of-sight would be slowed down more than in the spherically symmetric case. The discrepancy would be further reduced if the nova shell is mainly slowed down in the momentum-conserving phase rather than the energy-conserving phase, which is made more likely in this asymmetric case where the mass is concentrated in the orbital plane. Exactly such an axisymmetric geometry and rapid deceleration is suggested by recent observations of RS Oph *(S47)*.

Indeed, the fact that there is neutral Na around the progenitor of SN 2006X requires cool material and suggests that the shell must have cooled down sufficiently and be in the momentum-conserving phase.

If the recurrent nova interpretation requires an aspherical geometry, then this implies that the apparent shell structure with the velocities we have observed would only be seen in SNe Ia which are observed close to the orbital plane of the system. This may be a useful future discriminant for this model. We also suggest that this interpretation is made more satisfying if the loss of the strong Na line at $\sim$40 km s^{-1} (components C and D in Fig. 2) is due to the interaction of the supernova ejecta with that nova shell, as that places a useful scale on the distance of the shell from the supernova. As a typical SN velocity of $\sim 10^4$ km s^{-1} is some 250 times faster than the shell, the interaction after 1 month corresponds to a recurrence time of $\sim$25 yr, which is a plausible value. The actual recurrence time could well be less, as that shell is not guaranteed to be the innermost shell, merely the innermost visible one.

As a check on the consistency of this model, we can combine our inferred electron density of $n_{\rm e} \sim 10^5$ cm^{-3} with the dimensions of the nova shell to produce an estimate of the mass of the shell:

$$\left(\frac{M_{\rm shell}}{M_\odot}\right) \sim 1.0 \times 10^{-7} \left(\frac{0.1}{X}\right) \left(\frac{\Delta r}{10^{13}\ {\rm cm}}\right) \left(\frac{n_{\rm e}}{10^5\ {\rm cm}^{-3}}\right) \left(\frac{r_{\rm shell}}{10^{15}\ {\rm cm}}\right)^2, \qquad \text{(S4)}$$

where, somewhat arbitrarily, we have taken a shell thickness (Δr) that is $\sim 1\%$ of the radius of the shell. Our greatest uncertainty is probably contained within the ionisation fraction X, which is needed to obtain the mass per free electron, though the quadratic dependence on $r_{\rm shell}$ alone leads to considerable uncertainty in the estimate of $M_{\rm shell}$. Note that we have assumed the shell is spherical; a wind concentrated in the equatorial plane may be ~ 10 times less massive.

If we assume that the mass in the shell is dominated by mass swept up from the wind (i.e. $\rm M_{wind} \gg M_{nova}$) and then take the shell radius to be the product of the recurrence time and shell velocity we can write:

$$\left(\frac{\dot{M}_{\rm wind}}{M_\odot/{\rm yr}}\right) \sim 2.5 \times 10^{-8} \left(\frac{0.1}{X}\right) \left(\frac{\Delta r}{10^{13}\ {\rm cm}}\right) \left(\frac{n_{\rm e}}{10^5\ {\rm cm}^{-3}}\right) \left(\frac{v_{\rm shell}}{50\ {\rm km/s}}\right)^2 \left(\frac{\Delta t_{\rm nova}}{10\ {\rm yr}}\right), \qquad \text{(S5)}$$

The wind loss rate derived in this way is consistent with our expectation in Equation S3.

References

S1. H. Dekker *et al.*, *Proc. SPIE* **4008**, 534 (2000).

S2. S. Vogt *et al.*, *Proc. SPIE* **2198**, 362 (1994).

S3. P. Ballester *et al.*, *The Messenger* **101**, 31 (2000).

S4. R.J. Rand, *Astrophys. J.* **109**, 2444 (1995).

S5. VPFIT has been developed by R.F. Carswell and can be freely downloaded at http://www.ast.cam.ac.uk/∼rfc/vpfit.html

S6. K. Krisciunas, private communication.

S7. L. Ferrarese *et al.*, *Astrophys. J.* **464**, 568 (1996).

S8. The Very Large Array telescope of the National Radio Astronomy Observatory is operated by Associated Universities, Inc. under a cooperative agreement with the National Science Foundation.

S9. P. Chandra, R. Chevalier, F. Patat, *ATel* **954** (2006).

S10. N. Panagia *et al.*, *Astrophys. J.* **469**, 396 (2006).

S11. R. Quimby, P. Brown, C. Gerardy, CBET **421** (2006).

S12. S. Benetti *et al.*, *Mon. Not. R. Astron. Soc.* **348**, 261 (2004).

S13. B. Canzian, R.J. Allen, *Astrophys. J.* **479**, 723 (1997).

S14. L.M. Hobbs, *Astrophys. J.* **191**, 381 (1974).

S15. J.T. Lauroesch, A.P.S. Crotts, J. Meiring, P. Kulkarni, D.E. Welty, D.G. York, CBET **421** (2006).

S16. R.M. Crutcher, *Astrophys. J.* **288**, 604 (1985).

S17. D.M. Meyer, M. Jura, *Astrophys. J.* **297**, 119 (1985).

S18. L. Wang, D. Baade, F. Patat, J.C. Wheeler, *CBET* **396** (2006).

S19. D. Lazzati, R. Perna, J. Flasher, V.V. Dwarkadas, F. Fiore, *Mon. Not. R. Astron. Soc.* **372**, 1791 (2006).

S20. H. Hao *et al.*, *Astrophys. J.* **659**, L99 (2007).

S21. N. Panagia, *Supernova 1987A: 20 Years after: Supernovae and Gamma-Ray Bursters*, S. Immler, R. McCray and K.W. Weiler, Eds. (AIP Conf. Proc., 2007), in press; preprint available online (http://arxiv.org/abs/0704.1666).

S22. D.A. Verner, G.J. Ferland, K.T. Korista, *Astrophys. J.* **465**, 487 (1996).

S23. W.A. Pauldrach *et al.*, *Astron. Astrophys.* **312**, 525 (1996).

S24. R.P. Kirshner *et al.*, *Astrophys. J.* **415**, 589 (1993).

S25. P.M. Vreeswijk *et al.*, *Astron. Astrophys.*, in press; preprint available online (http://arxiv.org/pdf/astro-ph/0611690).

S26. I.A. Crawford, *Mon. Not. R. Astron. Soc.* **328**, 1115 (2001).

S27. I. Appenzeller *et al.*, *The Messenger* **94**, 1 (1998).

S28. Data were obtained with ESO Telescopes at the Paranal Observatory under programme ID 063.H-0650(A), P.I. B. Leibundgut.

S29. C. Pavlovsky *et al.*, Advanced Camera for Surveys Instrument Handbook for Cycle 16, Version 7.1 (STScI, Baltimore, 2006).

S30. Images were retrieved from the data archive at the Space Telescope Institute. STScI is operated by the association of Universities for Research in Astronomy, Inc. under the NASA contract NAS 5-26555. Data were originally obtained by A. Crotts et al.

S31. S. D'odorico *et al.*, *Astron. Astrophys.* **215**, 21 (1989).

S32. R.J. Cumming *et al.*, *Mon. Not. R. Astron. Soc.* **283**, 1355 (1996).

S33. J. Sollerman *et al.*, *Astron. Astrophys.* **429**, 559 (2005).

S34. S. Mattila *et al.*, *Astron. Astrophys.* **443**, 649 (2005).

S35. M.M. Phillips *et al.*, *Astron. J.* **103**, 1632 (1992).

S36. S. Jha, P. Garnavich, P. Challis, R.P. Kirshner, *IAU Circ.*, No. 7054 (1998).

S37. D. Enard, *Proc. SPIE* **331**, 232 (1982).

S38. A. Kaufer *et al.*, *The Messenger* **95**, 8 (1999).

S39. D.V. Bowen, K.C. Roth, D.M. Meyer, J.C. Blades, *Astrophys. J.* **536**, 225 (2000).

S40. A. Fassia *et al.*, *Mon. Not. R. Astron. Soc.* **325**, 907 (2001).

S41. I. Hachisu, M. Kato, *Astrophys. J.* **558**, 323 (2001).

S42. W.M. Wood-Vasey, J.L. Sokoloski, *Astrophys. J.* **645**, L53 (2006).

S43. S.R. Pottash, *Bull. Astr. Inst. Netherlands* **19**, 227 (1967).

S44. R.M. Hjellming *et al.*, *Astrophys. J.* **305**, L71 (1986).

S45. L. Sedov, *Similarity and Dimensional Methods In Mechanics* (Academic Press, New York, 1959).

S46. O. Yaron, D. Prialnik, M.M. Shara, A. Kovetz, *Astrophys. J.* **623**, 398 (2005).

S47. T.J. O'Brien *et al.*, *Nature* **442,** 279 (2006).